Influence of Solvent Effects on the Basicity of Pentaammine(pyrazine)ruthenium(II) and Pentacyano(pyrazine)ruthenate(II) Ions: A Density Functional Study

O. Yasmine Hamra, Leonardo D. Slep, José A. Olabe, and Darío A. Estrin*

Departamento de Química Inorgánica, Analítica y Química Física, and INQUIMAE, Facultad de Ciencias Exactas y Naturales, Universidad de Buenos Aires, Ciudad Universitaria, Pabellón 2, 1428 Buenos Aires, Argentina

Received September 3, 1997

Quantum chemical calculations using density functional theory have been carried out to investigate the basicity of pentaammine(pyrazine)ruthenium(II) and pentacyano(pyrazine)ruthenate(II) ions. Gas phase equilibrium geometries were fully optimized at the local density approximation (LDA) level. Single-point calculations were performed at the optimized gas phase geometries using a generalized gradient approximation (GGA) functional. The basicity of the uncoordinated nitrogen on pyrazine was investigated in gas phase and in aqueous solution, modeling solvent effects using a self-consistent reaction field (SCRF) Onsager model, a discrete electrostatic representation of the water molecules in the first solvation shell, and also a combined SCRF−discrete model within the DFT−GGA methodology. A reasonable level of agreement between theory and experiment is obtained only when using the SCRF−discrete model, suggesting that both specific interactions in the first solvation shell and long-range dielectric effects affect the reactivity of the complexes.

Introduction

The interpretation of experimental results on the structure, spectroscopy and reactivity of transition metal compounds has been successfully aided by the use of theoretical models and modern computational techniques.[1] This is particularly true for coordination compounds which can be considered as isolated species in condensed phases, i.e., weakly interacting with the medium, as in the case of many organometallic compounds or complexes containing ligands such as carbonyl or polypyridines, showing no tendency to engage in specific, donor−acceptor interactions with the solvent or other species such as counterions. On the other hand, the so-called "second-sphere" interactions have been shown to influence strongly the chemical properties of species in the first coordination sphere of some compounds leading to solvatochromic shifts in the charge-transfer absorption bands, as well as in the redox potentials associated to the metal centers.[2] The theoretical modeling of these systems is a challenging issue indeed since solvation effects should be taken into account.

In a previous work,[3] we used density functional theory (DFT) to study the electronic structure of $[Fe(CN)_5NO]^{2-}$ dissolved in different media. The calculations showed a good agreement with experimental data obtained in nonacceptor, aprotic solvents; in aqueous solutions, however, deviations were found that could not be accounted for by the dielectric continuum model used. The properties of the NO ligand were strongly influenced by the specific interactions of cyanides with the solvent, leading to internal electronic shifts favored by the coupled cyanide−iron−nitrosyl framework.

The occurrence of specific donor−acceptor interactions between cyanides and the solvent is not only characteristic of $[Fe(CN)_5NO]^{2-}$ but also of other $[M^{II}(CN)_5L]^{n-}$ complexes (M = Fe, Ru, Os; L = pyridine (py), pyrazine (pz), and *N*-methylpyrazinium ($mepz^+$)).[4,5] In addition to the structural parameters, Mulliken population analysis provide useful indicators of the trends in the back-bonding abilities of iron (as well as ruthenium) toward the three acceptor ligands.[5] These pentacyano−L ions have been extensively used in studies of the structure and reactivity of pseudooctahedral species, thanks to the availability of compounds for the three transition series, the ability of M to reach oxidation states II and III, and the widely accessible disposal of L ligands.[6] This is also the case with the $[M^{II}(NH_3)_5L]^{n+}$ series (M = Ru, Os).[7] Thus, also the influence of the coligands cyanide and ammine (or others) on the properties of the complex, particularly of the M−L bond, has been investigated. It is remarkable that for the $[M^{II}(NH_3)_5L]^{n+}$ series specific interactions with the solvents also exist, although now the ammines and the solvents interact as acceptor and donor, respectively.[7a]

The aim of the present work was to account for the solute−water interactions in the theoretical calculation by an adequate

* To whom correspondence should be addressed. E-mail: dario@q1.fcen.uba.ar.

(1) (a) Salahub, D. R.; Fournier, R.; Mlynarski, P.; Papai, I.; St-Amant, A.; Ushio, J. In *Theory and Applications of Density Functional Approaches in Chemistry*; Labanowski, J., Andzelm, J., Eds.; Springer-Verlag: Berlin, 1990. (b) Ziegler, T. *Chem. Rev.* **1991**, *91*, 651. (c) Sosa, C.; Andzelm, J.; Elkin, B. C.; Wimmer, E.; Dobbs, K. D.; Dixon, D. A. *J. Phys. Chem.* **1992**, *96*, 6630.
(2) Balzani, V.; Sabbatini, N.; Scandola, F. *Chem. Rev.* **1986**, *86*, 319.
(3) Estrin, D. A.; Baraldo, L. M.; Slep, L. D.; Barja, B. C.; Olabe, J. A. *Inorg. Chem.* **1996**, *35*, 3897.
(4) (a) Toma, H. E.; Takasugi, M. S. *J. Solution Chem.* **1983**, *12*, 547. (b) Toma, H. E.; Takasugi, M. S. *J. Solution Chem.* **1989**, *18*, 575. (c) Timpson, C. J.; Bignozzi, C. A.; Sullivan, B. P.; Kober, E. M.; Meyer, T. J. *J. Phys. Chem.* **1996**, *100*, 2915. (d) Slep, L. D.; Baraldo, L. M.; Olabe, J. A. *Inorg. Chem.* **1996**, *35*, 6327. (e) Waldhoer, E.; Kaim, W.; Olabe, J. A.; Slep, L. D.; Fiedler, J. *Inorg. Chem.* **1997**, *36*, 2969.
(5) Estrin, D. A.; Hamra, O. Y.; Paglieri, L.; Slep, L. D.; Olabe, J. A. *Inorg. Chem.* **1996**, *35*, 6832.
(6) Macartney, D. H. *Rev. Inorg. Chem.* **1988**, *9*, 101.
(7) (a) Curtis, J. C.; Sullivan, B. P.; Meyer, T. J. *Inorg. Chem.* **1983**, *22*, 224. (b) Creutz, C.; Chou, M. H. *Inorg. Chem.* **1987**, *26*, 2995. (c) Lay, P. A.; Harman, W. D. *Adv. Inorg. Chem.* **1991**, *37*, 219.

S0020-1669(97)01122-1 CCC: $15.00
Published on Web 04/01/1998

modeling of the "interplay" between the first coordination sphere and the bulk. We deal with a particularly useful indicator of the L ligand reactivity in the $[Ru^{II}(NH_3)_5L]^{n+}$ and $[Ru^{II}(CN)_5L]^{n-}$ systems, namely the basicity, as given by the free energy change for the protonation reaction at the uncoordinated nitrogen of L = pz. The experimental values of pK_a for the $[Ru(NH_3)_5pzH]^{3+}$ and the $[Ru(CN)_5pzH]^{2-}$ ions in aqueous solution have been widely used as indicators of the corresponding back-bonding abilities of ruthenium, as a result of the different coligands.[8] Through the present calculations, we search on the influence of solvation on the solution basicities, to probe the assertion that not only "internal" factors, such as the nature of the metal or the coligands, are crucial for the interpretation of experimental pK_a values.

Computational Methodology

The calculations were performed using the Molecole-DFT program.[9] The Kohn−Sham self-consistent procedure was applied for obtaining the electronic density and energy through the determination of a set of one-electron orbitals.[10] Gaussian basis sets were used for the expansion of the one-electron orbitals and also for the additional auxiliary set used for expanding the electronic density. Matrix elements of the exchange-correlation potential were calculated by a numerical integration scheme.[11] The orbital and auxiliary basis sets optimized by Sim et al.[12] for DFT calculations were used for C, N, and H atoms. For Ru, the basis sets given in ref 13 were used. The contraction patterns were (5211/411/1) for C and N, (633321/53211/531) for Ru, and (41/1) for H. The contraction patterns for the electronic density expansion sets are (1111111/111/1) for C and N, (1111111111/11111/11111) for Ru, and (111111/1) for H. A more detailed description of the technical aspects of the program is given in ref 9.

Geometries were optimized for the isolated systems within the local density approximation (LDA), using the Vosk−Wilk−Nusair correlation functional.[14] It has been shown that LDA is as good as GGA for computing metal−ligand geometries in Werner-type transition metal complexes.[15] This can be ascribed to the compensation of errors related to the LDA tendency to overbind and to the neglect of relativistic effects in Ru complexes. Single-point calculations were performed at the LDA gas phase optimized geometries using the Becke and Perdew combination of functionals for exchange and correlation, respectively.[16,17] This level of theory has proved to be necessary for accurate evaluation of gas phase proton affinities within DFT, since LDA yields systematically underestimated values.[18]

Although the most obvious way to account for solute−solvent interactions in a theoretical calculation is to surround the molecule of interest with sufficient solvent molecules to represent the effects of bulk solvation, this approach is extremely expensive if electronic structure calculations are performed in the full system. Different continuum models have been successfully used for the calculation of ligand exchange reactions and electrode potentials;[19] however, as mentioned above, they may show deviations in cases in which specific interactions are important. We have implemented a hybrid discrete approach, by treating the solute quantum mechanically and the remainder of the system by using classical force fields. Communication between the two parts of the system is allowed via electrostatic and van der Waals interactions. Several of these hybrid potentials have been implemented using semiempirical, ab initio, and DFT methods.[20] Within this scheme, we consider explicitly only the first shell of water molecules. In addition, and in order to take into account long-range electrostatic effects, we have considered the whole solute−solvent system as surrounded by a continuum having the dielectric constant of bulk water. This methodology allows the discrimination between specific and long-range solvent effects, even if is not intended to be quantitatively accurate.

The Onsager reaction field model[21,22] with a spherical cavity was used for modeling the dielectric interactions. The solvent was considered as a uniform dielectric, characterized by a given dielectric constant ϵ. The dipole of the solute induces a dipole (reaction field) in the solvent, which in turn interacts with the molecular dipole. The reaction field was updated iteratively until self-consistency was achieved. The only adjustable parameter in the Onsager's SCRF model is the radius of the spherical cavity (a_0). It can be evaluated in several ways: one recipe is based on estimating it from the experimental molecular volume, which can be obtained from the density. An alternative method consists of estimating the value of a_0 from the larger internuclear distance, adding the van der Waals radii of the atoms involved.

A quantum mechanical recipe, proposed by Frisch and co-workers, is based on computing the 0.001 au electron density envelop of the gas phase geometry and applying a scaling factor of 1.33 to obtain an estimate of the molecular volume and finally adding a value of 0.5 Å to the calculated radius a_0 in order to account for the nearest approach of solvent molecules.[23] This recipe has been shown to provide reasonable estimates of a_0 and has the advantage that no experimental information is required, so it has been used in the present work. The reaction field calculations were performed at the gas phase optimized geometries. This crude model is not expected to account for specific interactions.

The first shell of water molecules was considered by using the hybrid discrete scheme described above, using the single-point charge (SPC) potential[24] for water. Structural changes in complex geometry due to the solvent were neglected. Since many structures of nearly the same total energy are possible, we considered "typical" solvation structures, consisting in six water molecules solvating $[Ru(CN)_5pz]^{3-}$ and $[Ru(CN)_5pzH]^{2-}$ and eleven water molecules solvating $[Ru(NH_3)_5pz]^{2+}$ and $[Ru(NH_3)_5pzH]^{3+}$. The water molecules in the first solvation shell were chosen such as to solvate each cyanide with one hydrogen bonded water molecule. The hydrogen bond distance ($N_{cyanide}-H_{donor}$) was taken as 1.5 Å. For $[Ru(NH_3)_5pz]^{2+}$, $[Ru(NH_3)_5pzH]^{3+}$, and related systems classical molecular dynamics simulations in water were reported in refs 25 and 26. Our proposed "frozen" solvation structures were taken to be consistent with the correlation functions generated by the simulations, i.e., two hydrogen-bonded waters were considered solvating each NH_3 with an hydrogen bond distance taken as 2.0 Å ($H_{ammonia}-O_{acceptor}$). One additional hydrogen-bonded water was considered solvating the uncoordinated N of pyrazine in the cyano and ammino complexes, taking the N−H donor distance as 1.75 Å. In the protonated systems, a water molecule was considered solvating the protonated nitrogen, with a H−O donor distance of 1.5 Å. The combined continuum−discrete scheme

(8) (a) Ford, P. C.; Rudd, D. P.; Gaunder, R.; Taube, H. *J. Am. Chem. Soc.* **1968**, *90*, 1187. (b) Johnson, C. R.; Shepherd, R. E. *Inorg. Chem.* **1983**, *22*, 1117.
(9) Estrin, D. A.; Corongiu, G.; Clementi, E. In *METECC, Methods and Techniques in Computational Chemistry*; Clementi, E., Ed.; Stef: Cagliari, 1993; Chapter 12.
(10) Kohn, W.; Sham, L. J. *Phys. Rev.* **1965**, *A140*, 1133.
(11) Becke, A. D. *J. Chem. Phys*. **1988**, *88*, 1053.
(12) (a) Sim, F.; Salahub, D. R.; Chin, S.; Dupuis, M. *J. Chem. Phys*. **1991**, *95*, 4317. (b) Sim, F.; St-Amant, A.; Papai, Y.; Salahub, D. R. *J. Am. Chem. Soc*. **1992**, *114*, 4391.
(13) Basis set obtained from http://www.cray.com/PUBLIC/APPS/UNICHEM.
(14) Vosko, S. H.; Wilk, L.; Nusair, M. *Can. J. Chem*. **1980**, *58*, 1200.
(15) Bray, M. R.; Deeth, R. J.; Paget, V. J.; Sheen, P. D. *Int. J. Quantum Chem.* **1996,** *61*, 85.
(16) Perdew, P. W. *Phys. Rev.* **1986**, *B33*, 8800; Erratum, *B34*, 7406.
(17) Becke, A. D. *Phys. Rev.* **1988**, *A38*, 3098.
(18) Chandra, A. K.; Goursot, A. *J. Phys. Chem.* **1996**, *100*, 11596.
(19) Wu, J. H.; Reynolds, C. A. *J. Am. Chem. Soc.* **1996**, *118*, 14899.
(20) a) Ho, L. L.; MacKerell, A. D.; Bash, P. A. *J. Phys. Chem.* **1996**, *100*, 4466. (b) Eurenius, K. P.; Chatfield, D. C.; Brooks, B. R. *Int. J. Quantum Chem*. **1996**, *60*, 1189.
(21) Onsager, L. *J. Am. Chem. Soc*. **1936**, *58*, 1486.
(22) Paglieri, L.; Corongiu, G.; Estrin, D. A. *Int. J. Quantum Chem*. **1995**, *56*, 615.
(23) Wong, M. W.; Wiberg, K. B.; Frisch, M. J. *J. Am. Chem. Soc*. **1992**, *114*, 1645.
(24) Berendsen, H. J. C.; Postma, J. P. M.; von Gunsteren, W. F.; Hermans, J. In *Intermolecular Forces*; Pullman, B., Ed.; Reidel: Dordrecht, 1981; p 331.
(25) Zeng, J.; Hush, N. S.; Reimers, J. R. *J. Am. Chem. Soc*. **1996**, *118*, 2059.
(26) Zeng, J.; Hush, N. S.; Reimers, J. R. *J. Phys. Chem*. **1995**, *99*, 10459.

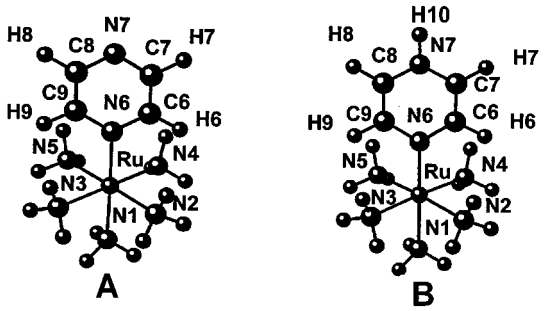

Figure 1. Structures of $[Ru(NH_3)_5pz]^{2+}$ (A) and $[Ru(NH_3)_5pzH]^{3+}$ (B) in a vacuum.

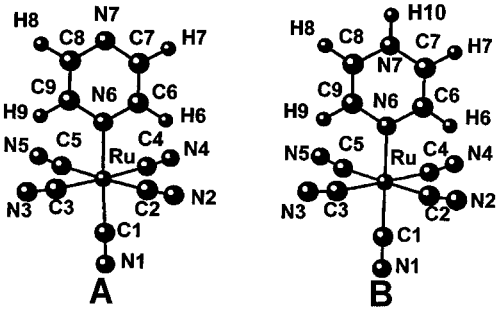

Figure 2. Structures of $[Ru(CN)_5pz]^{3-}$ (A) and $[Ru(CN)_5pzH]^{2-}$ (B) in a vacuum.

consisted in using the discrete solvated structures described above interacting with the reaction field of the solvent, treated with the Onsager's spherical cavity model, with the value of a_0 of the pure continuum calculation.

Results and Discussion

Gas Phase Optimized Structures. Figures 1A and 2A show the optimized geometries for the $[Ru(NH_3)_5pz]^{2+}$ and the $[Ru(CN)_5pz]^{3-}$ ions; in side B, we include the corresponding structures for the pyrazine-protonated species. The geometries of the ammine complexes are approximately octahedral. The heterocycle rings are essentially planar and oriented such that they bisect the N2−Ru−N4 and N3−Ru−N5 bond angles in both cases. The cyanide complexes are also close to octahedral and the heterocyclic rings are again planar. The plane of the ring intersects at a 45° angle, the equatorial plane containing the N atom of the heterocycle and the three atoms of the cyanide groups, as predicted by stereochemical considerations.

Table 1 shows the relevant bond distances (computed and experimental) for the unprotonated pentaammine species, as well as computed values for the pyrazine-protonated species.

The calculated results for $[Ru(NH_3)_5pz]^{2+}$ compare well with the experimental X-ray data for $[Ru(NH_3)_5pz](BF_4)_2$.[27] The rms deviation for the optimized metal−ligand bond distances is 0.029 Å. It can be seen that the experimental Ru−N(6) and Ru−N(1) distances are shorter than the calculated ones, while the equatorial Ru−N distances are longer. The shifts are probably associated to the donor influence of the BF_4^- counterions in the solid, which make the complex more electron rich along the Ru−pz axis, thus strengthening the trans Ru−NH_3 bond as well as the Ru−N(pz) bond. The interpretation is consistent with the known ability of bound ammine ligands in Ru(II) complexes to engage in specific interactions with donor solvents.[7a] Besides, it can be seen that the Ru−N(6) bond length (both calculated and experimental) is the shortest one, as expected from the contribution of back-donation from ruthenium to the π^*(pz) orbital.

Table 1. Computed Bond Distances (Å) for $[Ru(NH_3)_5pz]^{2+}$ and $Ru(NH_3)_5PzH]^{3+}$ in Vacuo

	pz	pz (expt)[a]	pzH^+
Ru−N(1)	2.176	2.166	2.169
Ru−N(2)	2.129	2.151	2.133
Ru−N(3)	2.124	2.149	2.133
Ru−N(4)	2.129	2.165	2.138
Ru−N(5)	2.133	2.145	2.141
Ru−N(6)	2.058	2.006	2.032
N(6)−C(6)	1.350	1.380	1.365
C(6)−C(7)	1.393	1.370	1.380
C(7)−N(7)	1.329	1.380	1.343
N(7)−C(8)	1.330	1.340	1.344
C(8)−C(9)	1.392	1.380	1.379
C(4)−N(6)	1.354	1.360	1.368
C(6)−H(6)	1.103		1.104
C(7)−H(7)	1.110		1.104
C(8)−H(8)	1.110		1.105
C(9)−H(9)	1.101		1.105
N(7)−H(10)			1.039

[a] Reference 27.

Table 2. Computed Bond Distances (Å) for $[Ru(CN)_5pz]^{3-}$ and $[Ru(CN)_5pzH]^{2-}$ in Vacuo

	pz	pzH^+		pz	pzH^+
Ru−C1	2.014	2.011	N6−C6	1.351	1.363
Ru−C2	2.061	2.055	C6−C7	1.384	1.360
Ru−C3	2.056	2.054	C7−N7	1.343	1.373
Ru−C4	2.061	2.055	N7−C8	1.343	1.371
Ru−C5	2.056	2.054	C8−C9	1.384	1.359
Ru−N6	2.057	1.998	C9−N6	1.356	1.369
C1−N1	1.184	1.179	C6−H6	1.106	1.102
C2−N2	1.185	1.180	C7−H7	1.108	1.101
C3−N3	1.184	1.180	C8−H8	1.109	1.101
C4−N4	1.185	1.181	C9−H9	1.110	1.104
C5−N5	1.184	1.180	N7−H(10)	1.024	

The Ru−N(pz) bond length decreases upon protonation, consistently with the stronger electron-withdrawing ability of protonated pyrazine, which causes an increase in back-donation. The Ru−N (NH_3) bond distances follow the same trends as discussed above; the stronger electron-withdrawing influence of pzH^+ compared to pz leads to similar shifts along the asymmetric axis as those observed upon the influence of donor counteranions.

Table 2 shows the calculated distances for the $[Ru(CN)_5pz]^{3-}$ and the $[Ru(CN)_5pzH]^{2-}$ species. No experimental data are available in the literature for the pyrazine−pentacyano complexes, but comparisons can be made with data published for $Na_4[Ru(CN)_6]\cdot 10H_2O$[28] and for $Na_2[Ru(CN)_5NO]\cdot 2H_2O$.[29] The average Ru−C distances in the latter compounds were 2.02 and 2.05 Å, respectively, and they compare well with calculated data in Table 2. The same can be said on the C−N distances (1.15−1.16 Å in the above compounds, respectively).

Upon protonation of pyrazine, the shifts in the distances are all consistent with the stronger electron-withdrawing ability of pzH^+ over pz, as discussed above with the ammine complex. Thus, the Ru−C bonds as well as the Ru−N(pz) bond become shorter. Also, the C−N bonds become slightly shorter, as expected from a lower population of the π^*(CN) orbitals (see below). The same trends in the C−N and C−C distances of the heterocyclic ring upon protonation observed in the ammine

(27) Gress, M. E.; Creutz, C.; Quicksall, C. O. *Inorg. Chem.* **1981**, *20*, 1522.
(28) Gentil, L. A.; Navaza, A.; Olabe, J. A.; Rigotti, G. E. *Inorg. Chim. Acta* **1991**, *179*, 89.
(29) Olabe, J. A.; Gentil, L. A.; Rigotti, G. E.; Navaza, A. *Inorg. Chem.* **1984**, *23*, 4297.

complex can be noticed in this case. Moreover, even the C−H distances show clearly a decreasing trend, as expected from a strengthening of the bonds due to the larger population of the bonding C−H orbitals.

Gas Phase Basicities. The acid−base protonation equilibria for $[Ru(CN)_5pz]^{3-}$ and $[Ru(NH_3)_5pz]^{2+}$ in gas phase are described by eqs 1 and 2.

$$[Ru(CN)_5pzH]^{2-} \rightarrow [Ru(CN)_5pz]^{3-} + H^+ \quad (1)$$

$$[Ru(NH_3)_5pzH]^{3+} \rightarrow [Ru(NH_3)_5pz]^{2+} + H^+ \quad (2)$$

The case of free pyrazine was also investigated (eq 3).

$$pzH^+ \rightarrow pz + H^+ \quad (3)$$

The proton affinities (PA) are defined as the enthalpy changes for reactions 1−3. The evaluation of proton affinities at 0 K involves computing the difference in electronic energies and zero-point energies (ZPE) between protonated and unprotonated species. Results at room temperature were estimated by adding thermal corrections to take into account the change in population of vibrational, rotational, and translational levels of protonated and unprotonated species and of the free proton with temperature, using standard formulas of statistical mechanics[30] and the rigid-rotor, harmonic oscillator, and ideal gas approximations.[31,32]

$$PA = \Delta E_0 + \Delta ZPE + \Delta H_v(T) + \Delta H_r(T) + \Delta H_t(T) \quad (4)$$

The first term (ΔE_0) was evaluated from the energy difference between protonated and unprotonated species in eqs 1−3. Since it is well established[18] that a satisfactory prediction of PA requires the use of gradient-corrected exchange and correlation functionals, single-point GGA calculations were carried out at the LDA-optimized geometries for protonated and unprotonated species in reactions 1−3. The other terms are the change in vibrational, rotational, and translational contributions to the enthalpy with temperature.

Because the evaluation of the vibrational frequencies necessary for the calculation of the second and third terms of eq 4 was too costly in reactions 1 and 2, both terms were estimated by performing a vibrational analysis in reaction 3. This estimation is reasonable because the most significant changes in vibrational modes upon protonation in reactions 1−2 are localized in the pyrazine ligand, especially in the high-frequency stretching mode $N_{pyrazine}$−H. This can be confirmed by the experimentally observed fact that M−C and C−N wavenumbers are almost independent of the sixth ligand L in the IR spectra of $[M(CN)_5L]^{n-}$ species, with L = N-heterocyclic ligand.[4d]

The gas phase free energy change can be evaluated by adding the thermal entropic contributions of protonated and unprotonated species and the free proton, estimated using the same approximations mentioned previously, based on equipartition of energy, rigid-rotor, and harmonic oscillator approximations.[32]

$$\Delta G_{gp} = PA - T\Delta S \quad (5)$$

In Table 3, results for proton affinities (PA) and gas phase free energy changes (ΔG_{gp}) at 298 K are presented for $[Ru(CN)_5pz]^{3-}$, free pz, and $[Ru(NH_3)_5pz]^{2+}$. Only the results for pz can be compared with experimental results, since the other two species exist only in solution. It is remarkable that in gas phase the $[Ru(NH_3)_5pz]^{2+}$ ion is found to be notably less basic than the $[Ru(CN)_5pz]^{3-}$ complex, in contrast to the experimental order of basicities in aqueous solution, as measured by the pK_a's (see below). Evidently, the chemistry of these compounds is profoundly influenced by the solvent. So the next step of our work consisted in the investigation of the influence of hydration on the basicity.

Table 3. Gas Phase Proton Affinities and Free Energy Changes[a]

	ΔE_o	PA	ΔG_{gp}
$[Ru(CN)_5pz]^{3-}$	422.4	415.5	407.7
pz	215.4	208.6	200.9
$[Ru(NH_3)_5pz]^{2+}$	94.6	87.7	80.0

[a] In kcal/mol. The zero-point energies (ΔZPE) = −8.3 kcal/mol for the cyano and ammonia complexes were taken as equal to the values obtained for free pyrazine.

Solution Basicities. The acid−base equilibria in solution can be described by

$$BH^+(aq) \rightarrow B(aq) + H^+(aq) \quad (6)$$

where B is the base and a solvated proton is used instead of the H_3O^+ ion. The use of the solvated proton may be justified since it is known that the hydronium ion is just part of a more extended hydration shell of the proton.[32] The change of standard free energy of process 6 is related to the pK_a by

$$\Delta G°/(RT \ln 10) = pK_a \quad (7)$$

Assuming that the standard free energy of protonation in gas phase (ΔG_{gp}) is known, it is necessary only to evaluate solvation free energies for the three species involved in reaction 6. Estimations of the free energy of the proton in water can be obtained from experimental data.[33] By including the translational free energy of the proton, a value of about −266 kcal/mol was estimated.[32]

Relative basicities can also be defined, to avoid using the experimentally derived free energy of the proton in water, which is still subject to controversies.

$$\Delta G' = \Delta G_{gp} + \Delta(\Delta G)_{sol} \quad (8)$$

where ΔG_{gp} is the free energy change in the gas phase and $\Delta(\Delta G)_{sol}$ is the difference in solvation free energies between the unprotonated and protonated species only.

$$\Delta(\Delta G)_{sol} = \Delta G_{solv.\ base} - \Delta G_{solv.\ prot} \quad (9)$$

We estimated the solvation free energies by using the three different solvation models described previously. In all cases the solute geometry in solution was assumed to be the same as in the gas phase. The nonelectrostatic contributions to the free energy of solvation such as cavitation and dispersion energies were neglected.[34] Since we are considering ionic systems in a polar solvent, we expect that electrostatic interactions represent the main part of solvation free energies. Table 4 shows the results for relative free energy changes ($\Delta G'$) and solvation free energies for protonated and unprotonated species.

First, we considered the continuum Born−Onsager spherical cavity model. In this simple approach, the leading part of the

(30) Hill, T. L. *An Introduction to Statistical Thermodynamics*; Dover Publications: New York, 1986.
(31) Curtiss, L. A.; Pople, J. A. *J. Phys. Chem.* **1988**, *92*, 894.
(32) Kallies, B.; Mitzner, R. *J. Phys. Chem. B* **1997**, *101*, 2959.
(33) Lim, C.; Bashford, D.; Karplus, M. *J. Phys. Chem.* **1991**, *95*, 5610.
(34) Cramer, C. J.; Truhlar, D. G. In *Quantitative Treatments of Solute/Solvent Interactions*; Politzer, P., Murray, J. S., Eds.; Elsevier Science: New York, 1994.

Table 4. Hydration Free Energies, ΔG_{solv}, and Relative Basicities $\Delta G'$ in Aqueous Solution Using Continuum, Discrete, and Discrete−Continuum Models[a]

	$[Ru(NH_3)_5pz]^{2+}$	$[Ru(CN)_5pz]^{3-}$	pz
	Continuum Model		
-ΔG solv. base	141.6	294.2	0.0
-ΔG solv. prot.	307.8	158.2	48.4
$\Delta G'$	246.0	271.7	249.3
	Discrete Model		
-ΔG solv. base	83.9	57.6	5.5
-ΔG solv. prot.	136.7	41.7	22.8
$\Delta G'$	132.8	391.8	218.2
	Discrete−Continuum Model		
-ΔG solv. base	227.9	354.2	5.6
-ΔG solv. prot.	444.0	211.6	72.6
$\Delta G'$	296.1	265.1	267.9
pK_a	2.5[b]	0.4[c]	0.6 [c]

[a] ΔG and $\Delta G'$ in kcal/mol. [b] Reference 8a. [c] Reference 8b.

solvation free energy in the case of ionic solutes is played by the net charge (Born's term), given by $-0.5Q^2/a_0(1 - 1/\epsilon)$, where Q is the system net charge, a_0 is the size of the cavity, and ϵ is the solvent dielectric constant. It can be seen that this model predicts that the solvation effects are responsible for the $[Ru(NH_3)_5pz]^{2+}$ complex becoming more basic than in the gas phase, since the protonated complex has a +3 charge, and the unprotonated +2; on the other hand, the $[Ru(CN)_5pz]^{3-}$ complex becomes less basic; here, the protonated species has a −2 charge, while the unprotonated one has a −3 charge. However, the model is unable to predict that the ammino complex is more basic than the cyano complex in aqueous solution, as observed experimentally; it accounts, however, for most of the differences between the results for isolated and hydrated systems.

We then performed a discrete first-shell calculation, representing the solvent molecules shell with the SPC model. These kind of models have been successfully used for predicting the spectroscopic properties of a related system, $[Ru(NH_3)_5py]^{2+}$, using a semiempirical approach for the electronic structure calculation.[35] Our calculations were done at a typical solvent configuration, as described above. A whole statistical treatment would be necessary to take into account thermal and entropic contributions to the standard free energy, so our "frozen solvation structure" calculation neglected such contributions. However, part of the errors are expected to cancel, since only differences in solvation free energy between the protonated and unprotonated complexes are evaluated. Comparatively, the continuum model provides us with a free energy of solvation which includes the entropy variation of the solvation process. Table 4 shows now that the $[Ru(NH_3)_5pz]^{2+}$ ion increases its basicity compared to the gas phase case. This fact can be explained in terms of the more favorable solvation of the protonated +3 system, due to the stronger H bonds formed between the NH_3 hydrogens with water molecules acting as donors, compared to the unprotonated complex. This is due to the larger positive charge that the ammonia hydrogens bear in the protonated system. The charges in the ammonia H atoms, given by a Mulliken population analysis of the isolated ion, range from 0.063 to 0.075 in the unprotonated complex and increase from 0.071 to 0.100 upon protonation. On the other hand, in the $[Ru(CN)_5pz]^{3-}$ complex, solvation favors the unprotonated species; since in that case the cyanides bear more negative charge and the hydrogen bonds between the cyanide terminal nitrogen atoms with the water molecules acting as acceptors are stronger than in the protonated case. The net charges on the cyanides, given also by a Mulliken population analysis, range from 0.595 and 0.637 in equatorial ligands and 0.830 in the axial cyanide and decrease to values ranging from 0.517 and 0.539 in equatorial ligands and 0.744 in the axial cyanide upon protonation. As a result, however, considering only these first-shell effects, the $[Ru(CN)_5pz]^{3-}$ complex is still predicted to be much more basic than the $[Ru(NH_3)_5pz]^{2+}$ complex, showing that the effects of solvation do not limit to the first solvation shell.

Finally, by using the mixed discrete-continuum calculation, in which both dielectric and first-shell solvation are taken into account, Table 4 shows that the qualitative trends in relative basicities are predicted correctly. Free pyrazine is predicted to be more basic than the $[Ru(CN)_5pz]^{3-}$ complex, and the $[Ru(NH_3)_5pz]^{2+}$ complex is predicted to be the most basic. By using the value of −266 kcal/mol for the free energy of the hydrated proton, we can compute pK_a values for free pyrazine and for $[Ru(CN)_5pz]^{3-}$ of 1.4 and −0.7, respectively, in fair agreement with the experimental ones, 0.65 and 0.3, respectively. This is not the case for $[Ru(NH_3)_5pz]^{2+}$, which is predicted to be much more basic than it really is. Probably, a main source of error relates to the first shell discrete solvent model used, particularly the neglect of entropic contributions to the solvation free energy as well as to the use of a mean-field nonpolarizable model for the water molecules. The lack of consideration of solvent polarization effects and the use of a potential parametrized for bulk pure water may cause an overestimation of solvation free energies. However, it is remarkable that consideration of solvent effects even at the level of the simple models used in this work brings the basicity ordering in agreement with experiment.

Orbital Populations. Table 5 shows the orbital populations for the ammonia and L (pz and pzH^+) ligands in the $[Ru(NH_3)_5pz]^{2+}$ (**A**) and $[Ru(NH_3)_5pzH]^{3+}$ (**B**) species. The results were obtained for the isolated species (vacuum), as well as for the different solvation models discussed in the previous section. In view of the good results obtained with the discrete-continuum model in the estimation of basicities, we compare now the results only for the latter approach with those from the vacuum calculations. It can be seen that the changes in the population of the σ(L), π(L), and $\sigma(NH_3)$ orbitals are small upon solvation of the ions ($\mathbf{A}_v \rightarrow \mathbf{A}_h$; $\mathbf{B}_v \rightarrow \mathbf{B}_h$) or upon protonation ($\mathbf{A}_v \rightarrow \mathbf{B}_v$; $A_h \rightarrow \mathbf{B}_h$). However, a significant increase in the population of π*(L) is obtained for any of the above processes. The calculations agree with experimental results showing that water engages in specific donor interactions with the $Ru^{II}(NH_3)_5L^{n+}$ species; also, protonation of pyrazine lowers the energy of π*(L) and a stronger back-bonding from Ru(II) is obtained.

With the $[Ru(CN)_5L]^{n-}$ species, Table 6 shows also that the main changes in population upon solvation or protonation are associated to the π*(L) orbital. Now, however, solvation ($\mathbf{A}_v \rightarrow \mathbf{A}_h$; $\mathbf{B}_v \rightarrow \mathbf{B}_h$) lowers the population of π*(pz), in contrast to the ammine complex, because water acts as an acceptor from donor cyanides. Protonation acts in the same sense as with the $[Ru(NH_3)_5pz]^{2+}$ species, i.e. the population of π*(L) increases, both in a vacuum and in the hydrated medium.

The changes in π*(L) populations upon solvation in both complexes are consistent with the predicted basicities. In vacuum, the π*(L) population in the cyano complex is much larger than the π*(L) population in the ammino complex (0.375 and 0.122, respectively), in agreement with the larger proton affinity of the former system. However, upon solvation the situation is reversed, since the π*(L) population of the ammino

(35) Stavrev, K. K.; Zerner, M. C.; Meyer, T. J. *J. Am. Chem. Soc.* **1995,** *117,* 8684.

Table 5. Ammonia and L Orbital Populations in $[Ru(NH_3)_5pz]^{2+}$ and $[Ru(NH_3)_5pzH]^{3+}$ (L = pz and pzH^+)[a]

	vacuum		continuum model		discrete model		discrete−continuum model	
	$\mathbf{A}_v$	$\mathbf{B}_v$	$\mathbf{A}_h$	$\mathbf{B}_h$	$\mathbf{A}_h$	$\mathbf{B}_h$	$\mathbf{A}_h$	$\mathbf{B}_h$
σ'(L)	1.903	2.000	1.908	2.000	1.890	1.977	1.895	2.000
π(L)	1.979	1.983	1.985	1.982	1.991	1.991	1.994	1.990
σ(L)	1.807	1.737	1.819	1.734	1.833	1.739	1.845	1.739
π*(L)	0.122	0.326	0.163	0.301	0.179	0.412	0.286	0.403
$\sigma(NH_3)_{eq}$	1.755	1.727	1.750	1.729	1.765	1.742	1.745	1.744
$\sigma'(NH_3)_{eq}$	1.967	1.959	1.964	1.960	1.967	1.966	1.959	1.967
$\sigma''(NH_3)_{eq}$	1.958	1.953	1.958	1.953	1.959	1.958	1.951	1.958
$\sigma(NH_3)_{eq'}$	1.753	1.720	1.748	1.722	1.753	1.726	1.737	1.725
$\sigma'(NH_3)_{eq'}$	1.954	1.958	1.951	1.958	1.959	1.953	1.952	1.952
$\sigma''(NH_3)_{eq'}$	1.972	1.950	1.969	1.951	1.959	1.961	1.960	1.961
$\sigma(NH_3)_{ax}$	1.768	1.729	1.740	1.738	1.795	1.753	1.747	1.757
$\sigma'(NH_3)_{ax}$	1.962	1.948	1.955	1.950	1.965	1.952	1.954	1.953
$\sigma''(NH_3)_{ax}$	1.968	1.961	1.962	1.963	1.963	1.954	1.955	1.955

[a] Key: $\sigma'(L) = \sigma(L)$ orbital of lower energy; $\sigma'(NH_3) = \sigma''(NH_3)$ orbital of lower energy; $\mathbf{A} = [Ru(NH_3)_5pz]^{2+}$; $\mathbf{B} = [Ru(NH_3)_5pzH]^{3+}$.

Table 6. Cyanide and L Orbital Populations in $[Ru(CN)_5pz]^{3-}$ and $[Ru(CN)_5pzH]^{2-}$ (L = pz and pzH^+)[a]

	vacuum		continuum model		discrete model		discrete −continumm model	
	$\mathbf{A}_v$	$\mathbf{B}_v$	$\mathbf{A}_h$	$\mathbf{B}_h$	$\mathbf{A}_h$	$\mathbf{B}_h$	$\mathbf{A}_h$	$\mathbf{B}_h$
σ'(L)	1.948	2.000	1.944	2.000	1.926	2.000	1.923	2.000
π(L)	1.984	1.981	1.990	1.986	1.986	1.984	1.991	1.987
σ(L)	1.829	1.765	1.831	1.760	1.848	1.766	1.844	1.757
π*(L)	0.375	0.872	0.232	0.549	0.347	0.753	0.209	0.413
$\sigma(CN)_{eq}$	1.403	1.384	1.405	1.389	1.478	1.466	1.481	1.468
$\pi(CN)_{eq}$	3.973	3.948	4.000	4.000	3.976	3.957	4.000	4.000
π*$(CN)_{eq}$	0.000	0.000	0.000	0.000	0.000	0.000	0.000	0.000
π'*$(CN)_{eq}$	0.146	0.124	0.149	0.131	0.143	0.118	0.146	0.134
$\sigma(CN)_{eq}$	1.384	1.382	1.388	1.389	1.477	1.462	1.480	1.469
$\pi(CN)_{eq'}$	3.977	3.946	4.000	4.000	3.981	3.959	4.000	4.000
π*$(CN)_{eq'}$	0.000	0.000	0.000	0.000	0.000	0.000	0.000	0.000
π'*$(CN)_{eq'}$	0.143	0.120	0.146	0.125	0.145	0.124	0.150	0.132
$\sigma(CN)_{ax}$	1.410	1.402	1.392	1.382	1.453	1.440	1.466	1.471
$\pi(CN)_{ax}$	3.964	3.925	3.959	3.936	3.979	3.950	3.968	3.946
π*$(CN)_{ax}$	0.170	0.179	0.160	0.195	0.121	0.130	0.132	0.164
π'*$(CN)_{ax}$	0.137	0.105	0.185	0.158	0.146	0.114	0.192	0.182

[a] Key: $\sigma'(L) = \sigma(L)$ orbital of lower energy; π'*(CN) = higher energy π*(CN) orbitals (11th, 12th, 14th, and 15th MO). $\mathbf{A} = [Ru(CN)_5pz]^{3-}$. $\mathbf{B} = [Ru(CN)_5pzH]^{2-}$.

complex is larger than the π*(L) population in the cyano complex (0.286 and 0.209, respectively).

Conclusions

Despite the simplicity of the solvation models considered in this work, they have been useful for explaining the main features of hydration in these systems, i.e.; long-range dielectric effects, mainly related to the global charges and dipole moments, and specific effects, related mainly to water−ligand local electrostatic interactions. The use of different solvation models, for example, continuum schemes in which the Poisson equation is solved exactly for a given charge distribution rather than using simplified approaches such as the Onsager−Born spherical cavity model, might shed light in the crude distinction made in this work of short-range ligand−solvent electrostatic interactions and global charges and dipole long-range effects. Work is in progress in these areas.

Leaving aside the consideration of solvation models, we conclude that accurate evaluation of solvation free energies is at least as important as making accurate electronic structure calculations in the isolated systems, to achieve the goal of using computational tools in the understanding of the structural and reactivity properties of many transition metal systems. In the case of the pentaammine(pyrazine)ruthenium(II) and pentacyano(pyrazine)ruthenate(II) investigated in this work this is most relevant for the properties associated to the sixth ligand L, namely the basicity of the exposed lone pair of pz and the population changes in the different orbitals. Similar conclusions can be drawn on the electrophilic reactivity for $L = NO^+$ in $[Fe(CN)_5NO]^{2-}$ whose dependence on the environment may be relevant to the physiological role of bound NO^+ in enzymes.[3] All of them demonstrate that, in addition to internal effects related to the type of metal and coligands, in these systems solvation also accounts for important features of the L ligand's reactivity.

Acknowledgment. This work was partially supported by the University of Buenos Aires. D.A.E and O.Y.H. acknowledge Fundación Antorchas for financial support. D.A.E. and J.A.O. are members of the scientific staff of CONICET (National Scientific Council of Argentina).

IC9711224